ACS APPLIED MATERIALS & INTERFACES

Research Article

www.acsami.org

Hexaphenylbenzene-Stabilized Luminescent Silver Nanoclusters: A Potential Catalytic System for the Cycloaddition of Terminal Alkynes with Isocyanides

Subhamay Pramanik, Vandana Bhalla,* and Manoj Kumar*

Department of Chemistry, UGC-Centre for Advanced Studies-II, Guru Nanak Dev University, Amritsar 143005, Punjab, India

Supporting Information

ABSTRACT: A hexaphenylbenzene (HPB)-based derivative bearing thiol groups has been designed and synthesized that undergoes aggregation-induced emission enhancement in mixed aqueous media to form rodlike fluorescent aggregates. These rodlike aggregates behave as a "not quenched" probe for the detection of silver ions and further act as reactors and stabilizers for reducing-agent-free preparation of blue luminescent silver nanoclusters at room temperature. The utilization of fluorescent supramolecular aggregates for the preparation of Ag NCs in mixed aqueous media is unprecedented in the literature. Moreover, the wet chemical method that we are reporting in the present paper for the preparation of luminescent silver nanoclusters is better than the other methods reported in the literature. Further, these in situ generated Ag NCs showed exceptional catalytic activity in the preparation of pyrroles involving cocyclization of isocyanides and terminal alkynes. Interestingly, the catalytic efficiency of in situ generated Ag NCs was found to be better than the other catalytic systems reported in the literature.

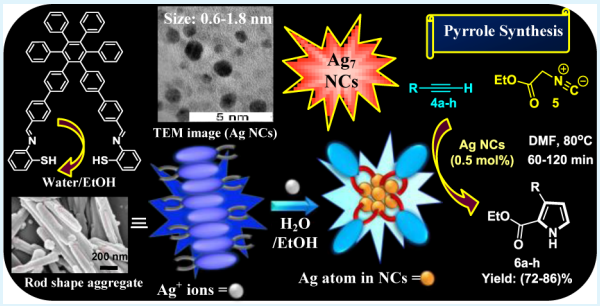

KEYWORDS: *hexaphenylbenzene, AIEE, luminescent silver nanoclusters, terminal alkyne, isocyanide, pyrrole*

1. INTRODUCTION

Pyrrole and its derivatives are of great use in organic synthesis and in material science. The five-membered heterocyclic core is a building block of various natural products, pharmaceuticals, agrochemicals, and alkaloids.[1] Thus, various approaches have been developed for the construction of pyrrole derivatives. The conventional methods for the synthesis of pyrroles require the presence of a strong base, expensive catalyst, and high temperature.[2] Recently, "click" reaction between terminal alkynes and isocyanides have been developed as a straightforward and convenient strategy for the development of pyrrole derivatives.[3] However, most of these reports suffer from limitations such as use of a high loading of expensive metal salts as catalyst, nonreusable catalyst, longer reaction time, and high reaction temperature.[4] Hence, the development of an efficient, atom-economic, and environmentally friendly approach for the preparation of pyrroles is still a challenge.

One of the aims of our research program is the development of fast, reductant-free, facile methods for the preparation of different types of metal nanoparticles, viz., palladium,[5] gold,[6] copper,[7] mercury,[8] and iron oxide.[9] The catalytic efficiency of these nanoparticles was then utilized for various organic transformation, viz., reduction of *p*-nitrophenol and *p*-nitroaniline to *p*-aminophenol[5] and *p*-phenylenediamine,[6] click synthesis of triazoles,[7] Beckmann rearrangement[8] of aldoximes/ketoximes to primary/secondary amides, and Sonogashira coupling[9] reactions, respectively. Recently, from our laboratory we reported the development of supramolecular assemblies based on different scaffolds, viz., pentacenequinone, hexaphenylbenzene, and perylenebisimide bearing aldehyde groups, which served as reactors and stabilizers for the preparation of nonluminescent silver nanoparticles (Ag NPs, size >2 nm).[10] However, nonluminescent Ag nanoparticles have limited applications, as these cannot be used for fluorescence lifetime imaging or tracking in live cells and are unable to exhibit fluorescence resonance energy transfer (FRET). Keeping this in view, we were then interested in the development of fluorescent supramolecular aggregates, which could act as reactors and stabilizers for the preparation of luminescent Ag NPs, and for this purpose, we have designed and synthesized hexaphenylbenzene (HPB) derivative **3**, having thiol groups at the periphery. We have chosen the HPB moiety because of its known aggregation-induced emission enhancement[11,12] (AIEE) characteristics in aqueous media. The soft imino and thiol groups have been incorporated to increase the affinity of the molecule toward soft metal ions like silver.[13] Interestingly, rodlike fluorescent supramolecular aggregates of HPB derivative **3** exhibited "no quenching" response toward silver ions in aqueous media and served as reactors and stabilizers for the preparation of very small silver nanoclusters (Ag_7 NCs, size ≤2

Received: May 20, 2015
Accepted: September 30, 2015
Published: September 30, 2015

DOI: 10.1021/acsami.5b04377
ACS Appl. Mater. Interfaces 2015, 7, 22786−22795

Table 1. Click Synthesis of Pyrroles by the Cocyclization of Terminal Alkynes (4a−h) and Ethyl 2-Isocyanoacetate (5) Catalyzed by Ag NCs (0.5 mol %)

Entry	Ethyl 2-isocyanoacetate, 5	Alkyne 4a-h	Time [h]	Product (Pyrrole derivatives) 6a-h	Isolated yield [%]
1	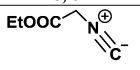	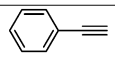 4a	2	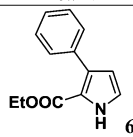 6a	80
2	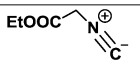	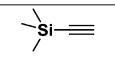 4b	1	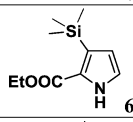 6b	75
3	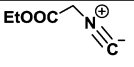	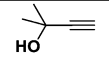 4c	1.2	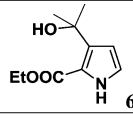 6c	85
4	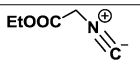	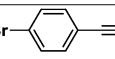 4d	2	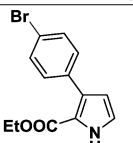 6d	78
5	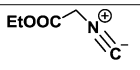	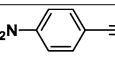 4e	1	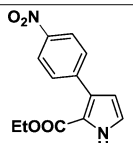 6e	72
6	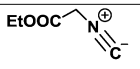	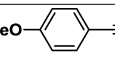 4f	1.2	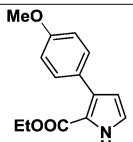 6f	80
7	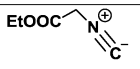	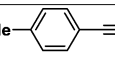 4g	2	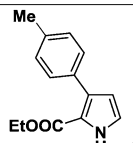 6g	86
8	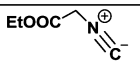	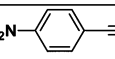 4h	2	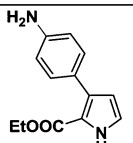 6h	82

nm) rather than Ag NPs. Among different metal nanoclusters, silver nanoclusters (Ag NCs), due to their exceptional photostability and bright fluorescence in solution phase, have found applications in biolabeling and FRET and for creating luminescent patterns.[14−27] Further, preparation of Ag NCs requires special efforts to avoid self-aggregation, which leads to the formation of nonfluorescent silver nanoparticles. In the recent past, various methods to produce luminescent Ag nanoclusters stabilized by a variety of protecting ligands such as polymers, dendrimers, peptides, and DNA oligonucleotides have been developed.[28−42] However, most of these methods have their own limitations of requiring photoirradiation,[43] an external reducing agent,[44,45] longer reaction time,[46] high temperature,[46,47] and incubation in dark.[31] In this context, the reductant-free wet chemical method that is being reported in the present paper for the preparation of luminescent Ag NCs is better than the other reported methods[28−47] (Supporting Information, Table S5). Furthermore, in situ generated, highly stabilized Ag NCs showed excellent catalytic efficiency in the preparation of pyrroles by click reaction (cocyclization) of isocyanides with terminal alkynes (Table 1). To the best of our knowledge, this is the first report where aggregates of a hexaphenylbenzene derivative have been utilized for the preparation of blue luminescent silver nanoclusters (Ag_7 NCs) that then have been used as a catalyst for the preparation of pyrrole derivatives by cocyclization of isocyanides with terminal alkynes. Interestingly, the catalytic efficiency of the Ag NCs was found to be better than the other catalytic systems reported in the literature (Supporting Information, Table S6).

2. RESULTS AND DISCUSSION

2.1. Synthesis and Characterization of HPB Derivative 3.

[1 + 2]-Condensation of hexaphenylbenzene derivative **1**[10] with 2-aminothiophenol **2** in THF:EtOH (4:6) at 80 °C afforded the desired product **3** in 89% yield (Scheme 1).

DOI: 10.1021/acsami.5b04377
ACS Appl. Mater. Interfaces 2015, 7, 22786−22795

Scheme 1. Synthesis of Hexaphenylbenzene-Based Derivative 3

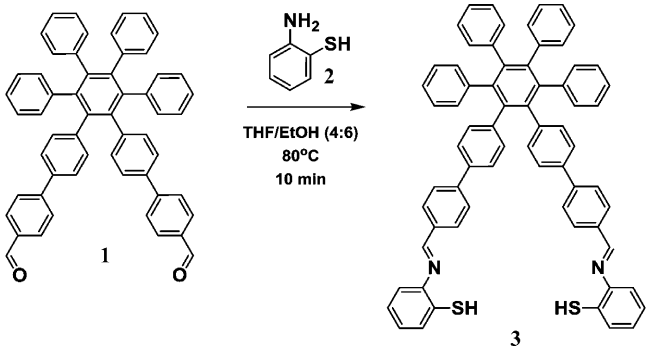

The structure of compound **3** was confirmed from its spectroscopic and analytical data (Supporting Information, Figures S30–33). The ^{1}H NMR spectrum of compound **3** showed two singlets at 8.78 and 3.52 ppm, corresponding to imino and SH proton, respectively; six doublets at 8.24, 8.07, 7.91, 7.59, 7.25, and 7.00 ppm; four triplets at 7.84, 7.50, 7.39, and 7.08; and a multiplet at 6.91–6.88 ppm, corresponding to aromatic protons. The ^{13}C NMR spectrum of **3** showed peaks at 160.9 and 156.7 ppm due to imino carbons and peaks at 143.2, 140.4, 136.8, 136.4, 132.1, 131.4, 130.1, 128.1, 127.8, 127.2, 126.8, 126.6, 125.6, 125.3, 123.1, and 118.2 ppm corresponding to other aromatic carbons. The FT-IR spectrum of compound **3** exhibits two distinct stretching bands at 1602 and 2580 cm^{-1} corresponding to the C═N and SH groups, respectively. In the ESI-MS spectrum of compound **3**, a base peak appeared at 979.4329 (m/z) corresponding to $[M + Na]^+$. These spectroscopic data confirm the structure **3** for this compound.

2.2. AIEE Behavior of Derivative 3. A solution of compound **3** in ethanol exhibits an absorption band at 324 nm due to the π–π^* transition in the UV–vis spectrum. On increasing water fractions up to 80% (volume fraction) to the ethanol solution, the entire absorption spectra gradually increased with a slight red shift (~6 nm) in the absorption band from 324 to 330 nm along with the appearance of a level-off tail in the visible region (Figure 1A). An emission band appeared at 385 nm (Φ = 0.06) in the fluorescence spectrum of a solution of compound **3** in ethanol when excited at 330 nm. On increasing the water fraction up to 80% (volume fraction) to the ethanol solution of **3**, the emission band is red-shifted to 405 nm with an enhancement in the emission intensity (Φ = 0.45) (Supporting Information, Figure S1A) and quantum yield (Φ) (Supporting Information, Figure S1B). The absorption and fluorescence studies suggest the formation of aggregates in mixed aqueous media. The shape of the aggregates was found to be rodlike, as observed in the scanning electron microscopic image (SEM) of derivative **3** in H_2O/EtOH (8:2, v/v) (Figure 1B,C and Supporting Information, Figure S2). The dynamic light scattering (DLS) studies also indicate the presence of rod-shaped aggregates of average length in the range of 600 nm (Supporting Information, Figure S3).

Further, the fluorescence intensity of compound **3** gradually increased with increasing fractions of glycerol in ethanol solution (Supporting Information, Figure S4). We also carried out concentration-dependent fluorescence studies of compound **3** in ethanol. These studies indicate nonlinear enhancement in fluorescence intensity with increasing concentration (Supporting Information, Figure S5). We also studied the effect of temperature on the fluorescence behavior of compound **3** in the H_2O/EtOH (8:2, v/v). It was found that the fluorescence intensity decreases gradually with the rise in temperature from 25 to 75 °C (Supporting Information, Figure S6). These studies confirm the aggregation-induced emission enhancement characteristics of derivative **3**.

The time-resolved fluorescence spectrum of derivative **3** in ethanol exhibits a single-exponential lifetime (τ = 0.37 ns), whereas upon addition of water fractions the fluorescence decay of derivative **3** becomes biexponential (τ_{avg} = 1.35 ns) (Supporting Information, Figure S7). These studies indicate that the difference between fluorescence radiative rate constants[47,48] (k_f) of derivative **3** in ethanol (0.16 × 10^9 s^{-1}) and in H_2O/EtOH (8:2, v/v) (0.33 × 10^9 s^{-1}) is very small; however, the nonradiative decay constant (k_{nr}) decreased significantly from 2.54 × 10^9 to 0.4 × 10^9 s^{-1} (Supporting Information, Table S1). On the basis of these studies, we propose that the deactivation of nonradiative decay due to restriction of the intramolecular rotational relaxation of the rotors linked to the core is the principal reason for the observed

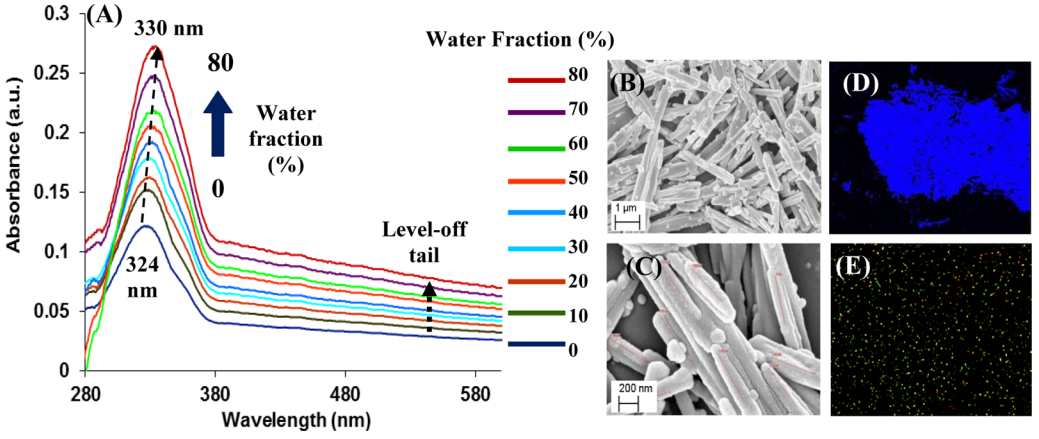

Figure 1. (A) UV–vis spectra showing the change in absorbance of compound **3** (5.0 μM) in H_2O/EtOH mixture (0–80% volume fraction of water in EtOH). The scanning electron micrographs showing the rod-shaped aggregates with scale bars of (B) 1 μm and (C) 200 nm. (D) Confocal image showing blue luminescent aggregates of **3**. (E) Polarized optical microscopic image of derivative **3** at room temperature through cross-polarizing filters.

DOI: 10.1021/acsami.5b04377
ACS Appl. Mater. Interfaces 2015, 7, 22786–22795

AIEE phenomena in the case of derivative **3**. The confocal microscopy image of compound **3** in the H_2O/EtOH (8:2, v/v) clearly indicates the presence of blue luminescent aggregates (Figure 1C). Furthermore, the polarized optical microscopy (POM) image of derivative **3** shows birefringence at room temperature, thus suggesting an ordered morphology (Figure 1D).

We also carried out concentration-dependent ^{1}H NMR studies of derivative **3**, which showed a downfield shift of 0.22 and 0.14 ppm for −SH and imino protons, respectively, indicating the presence of intermolecular hydrogen bonding between the molecules of derivative **3**. Further, an average upfield shift of 0.08 ppm was observed in the case of protons corresponding to the HPB moiety (Supporting Information, Figure S8). This upfield shift of aromatic protons is attributed to the intermolecular $\pi-\pi$ stacking between the HPB-based molecules. All these studies clearly indicate the AIEE characteristics of derivative **3**.

2.3. Preparation of Silver Nanoclusters Utilizing Aggregates of Derivative 3. Since compound **3** contained imine and thiol moieties, which are known to have interaction with metal ions, we studied the molecular recognition behavior of compound **3** with different metal ions, such as Ag^+, Hg^{2+}, Au^{3+}, Zn^{2+}, Cu^{2+}, Fe^{2+}, Fe^{3+}, Co^{2+}, Pb^{2+}, Ni^{2+}, Pd^{2+}, Cd^{2+}, Ba^{2+}, Mg^{2+}, and Al^{3+}, as their perchlorate/chloride and nitrate salts ($AgNO_3$) by UV−vis and fluorescence spectroscopy (Supporting Information, Figures S9 and S10). Upon gradual addition of Ag^+ ions (0−60 equiv) to the solution of **3** (5 μM) in H_2O/EtOH (8:2, v/v), the absorption band at 330 nm is gradually blue-shifted to 300 nm within the first 30 min due to the interaction of aggregates of derivative **3** with Ag^+ ions (Figure 2).[49] Interestingly, after 30 min, the formation of new bands

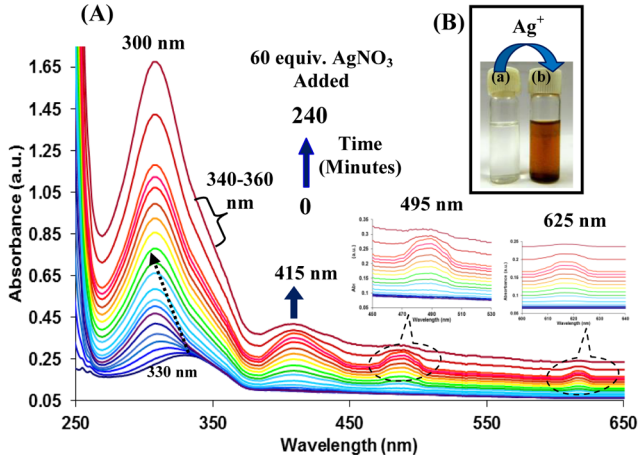

Figure 2. (A) UV−vis spectra of compound **3** (5.0 μM) in H_2O/EtOH (8:2, v/v) in the presence of Ag^+ ions (0−60 equiv) within 240 min; the inset shows the enlarged absorption bands at 495 and 625 nm. (B) Color change from colorless to yellow 240 min after of addition of 60 equiv of Ag^+ ions.

was observed at 415, 495, and 625 nm in the UV−vis spectra. The intensity of the bands at 415, 495, and 625 nm gradually increased with time (up to 240 min) (Figure 2A).

The band at 625 nm may be attributed to the interplasmon coupling[50] and interband transitions (4d valence band to the 5sp conduction band) during Ag NCs formation, and the broad band in the 340−360 nm region also suggests the formation of heptamer silver (Ag_7) nanoclusters.[51] Thus, the bands at 415, 495, and 625 nm and broad band in the 340−360 nm region indicate the formation of Ag_7 NCs.[52,53] A color change from colorless to yellow observable to the naked eye accompanied these spectral changes (Figure 2B). The rate constant for the formation of Ag NCs was found to be 5.55×10^{-3} min^{-1} (Supporting Information, Figure S11).

2.4. Luminescence Behavior of Silver Nanoclusters. Upon addition of Ag^+ ions (60 equiv) to the solution of aggregates of **3**, the emission band at 405 nm gradually decreases and red shifts to 415 nm within 60 min (Figure 3A). This red shift in emission band is attributed to the interactions between the aggregates of derivative **3** and Ag^+ ions.[54,55] After 60 min of Ag^+ ions addition, a new band appeared at 465 nm, and its emission intensity gradually increased (Φ = 0.66, 240 min) (Supporting Information, Figures S12 and S13) accompanied by a color change from deep blue to blue-green, which is clearly visible to the naked eye under 365 nm UV light (Figure 3A, inset). On the other hand, the fluorescence spectra of derivative **3** in the presence of Ag^+ ions also showed an emission band at 465 nm upon excitation at three different wavelengths (340, 350, and 360 nm) (Supporting Information, Figure S14). Further, we recorded the excitation spectrum of the solution of aggregates of **3** and Ag^+ ions for the emission at 465 nm. The excitation spectrum of the emission at 465 nm showed a broad peak at 345 nm, which overlaps significantly with the UV−vis absorbance and excitation (λ_{ex} = 330 nm) spectrum, suggesting that Ag NCs are contributing to the emission enhancement at 465 nm (Supporting Information, Figure S15).[27,47,56] A linear quenching efficiency plot was obtained in the case of aggregates of derivative **3** in the presence of Ag^+ ions (60 equiv) with a Stern−Volmer constant (K_{sv}) of 5.6×10^4 M^{-1} (Supporting Information, Figure S16). The detection limit of aggregates of derivative **3** for Ag^+ ions was found to be 150 nM (Supporting Information, Figure S17). We also tested the fluorescence behavior of aggregates of derivative **3** toward other metal ions, such as Hg^{2+}, Au^{3+}, Zn^{2+}, Cu^{2+}, Fe^{2+}, Fe^{3+}, Co^{2+}, Pb^{2+}, Ni^{2+}, Cd^{2+}, Pd^{2+}, Ba^{2+}, Mg^{2+}, and Al^{3+} ions, as their chloride (silver as $AgNO_3$) and perchlorate salts under the same conditions as used for Ag^+ ions, but no considerable change in fluorescence intensity was observed (Supporting Information, Figures S18 and S19), which indicates that the aggregates of derivative **3** are selective for Ag^+ ions only. This selectivity is due to the presence of soft imino and thiol moieties in derivative **3**, which interact selectively with soft Ag^+ ions among various other metal ions tested.[57]

We also studied the interaction between silver ions and derivative **3** by time-resolved fluorescence spectroscopy (Supporting Information, Figure S20). In the absence of Ag^+ ions, derivative **3** exhibits a biexponential lifetime (11%, τ_1 = 0.69 and 89%, τ_2 = 1.99 ns) in H_2O/EtOH (8:2, v/v) when measured at 465 nm, whereas in the presence of Ag^+ ions (60 equiv) after 60 min, the fluorescence decay of derivative **3** becomes triexponential. This result indicates the formation of additional unique species in the presence of Ag^+ ions. Further, after 60 min, the amplitude of the shorter component gradually decreased (1.15%, τ_1 = 0.33; 5.21%, τ_2 = 1.15 ns), whereas the amplitude of the longer component dramatically increased (93.64%, τ_3 = 11.7 ns).[58] Additionally, in the presence of Ag^+ ions, the major fraction (93.64%) of the molecules decay through the slower pathway (τ_3) due to the significant decrease in the nonradiative rate constant (Supporting Information, Table S2). The enhancement in decay rate may be attributed to

DOI: 10.1021/acsami.5b04377
ACS Appl. Mater. Interfaces 2015, 7, 22786−22795

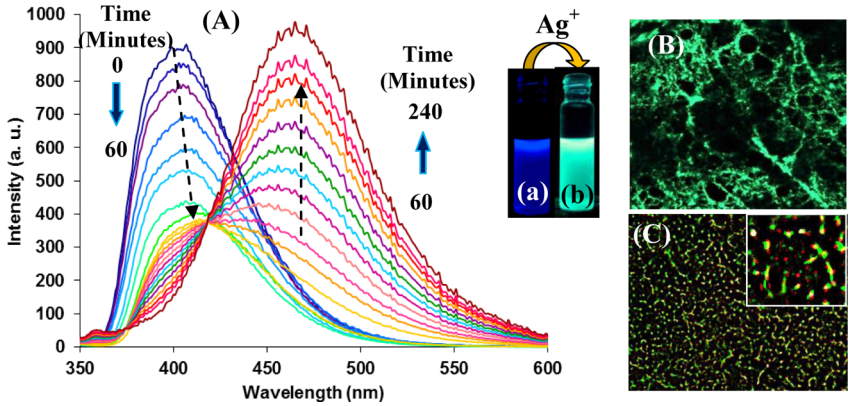

Figure 3. (A) Fluorescence spectra of compound **3** (5 μM) showing the response to the Ag^+ ions (0−60 equiv) in H_2O/EtOH (8:2, v/v) mixture buffered with HEPES (pH 7.05 and λ_{ex} = 330 nm); the inset shows the fluorescence change of **3** before (a) and after (b) the addition of Ag^+ ions (60 equiv, 240 min). (B) Confocal image showing green luminescent Ag_7 NCs. (C) Polarized optical microscopic image of derivative **3** in the presence of Ag^+ ions at room temperature through cross-polarizing filters; the inset shows the formation of silver nanoclusters by aggregates of **3**.

the increase in the radiative rate by the local field enhancement of the silver nanoclusters.

The image of compound **3** under the confocal microscope in H_2O/EtOH (8:2, v/v) in the presence of silver ions clearly indicates the presence of green luminescent particles (Figure 3B).[50,53] Furthermore, the image of compound **3** under polarized optical microscope (POM) containing Ag NCs showed greenish yellow birefringence (Figure 3C). These results clearly indicate the formation of luminescent Ag NCs. Further, the in situ generated Ag NCs are visibly stable at room temperature for several weeks.

2.5. Characterization of Silver Nanoclusters (Ag_7 NCs).

To get further insight into the mechanism and the effect of ligand concentration on the formation of silver nanoclusters, we carried out FT-IR, DLS, high-resolution transmission electron microscopic (HRTEM), and powder X-ray diffraction (XRD) studies of aggregates of derivative **3** in the presence of Ag^+ ions by mixing them in 1:1 and 1:2 ratio, respectively. The FT-IR spectrum of the sample obtained after evaporation of the solution of derivative **3** and Ag^+ ions mixed in 1:1 ratio showed a shift in peak corresponding to thiol groups from 2580 to 2549 cm^{-1} (Supporting Information, Figure S21a,b). On the other hand, the IR studies of the same sample prepared by mixing **3** and Ag^+ ions in 1:2 ratio showed the absence of a peak at 2580 cm^{-1} corresponding to thiol groups and a shift in the peak corresponding to imino groups from 1602 to 1585 cm^{-1}, which clearly indicates the interaction of silver ions with compound **3** through sulfur and imino nitrogen atoms (Supporting Information, Figures S21c and S22). Further, in the ^1H NMR spectrum of this sample, the peak at 3.52 ppm corresponding to thiol groups disappeared and an average upfield shift of 0.14 ppm was observed in the signals corresponding to imino protons and aromatic protons (Supporting Information, Figure S23 and Table S3).

On the basis of these results, we believe that upon addition of Ag^+ ions to the solution of aggregates of **3** in 1:2 ratio, Ag^+ ions interact with the sulfur and imino nitrogen atoms of compound **3** to enter into a network of interconnected aggregates and get reduced to Ag(0), and S−Ag covalent bonds were formed in the nanoclusters.[50,59,60] Further, the DLS studies of the sample obtained by mixing aggregates of **3** and Ag^+ ions in 1:1 ratio showed the presence of Ag NCs in the range of 4 nm (Supporting Information, Figure S24a); however, the DLS studies of sample obtained by mixing **3** and Ag^+ ions in 1:2 ratio showed the presence of much smaller sized particles having a hydrodynamic diameter in the range of 0.4−1.8 nm (average diameter ∼1 nm) (Supporting Information, Figure S24b).[61,62] The powder XRD pattern of the sample with 1:1 ratio of aggregates of derivative **3** and Ag^+ ions showed sharp peaks as the larger particles (4.0 nm) show a distinct diffraction pattern (Supporting Information, Figure S25c). However, the XRD of the sample with 1:2 ratio of aggregates of derivative **3** and Ag^+ ions showed the presence of broad peaks in the range of 10°−30° (2θ values) corresponding to derivative **3** with the broad peaks located at 2θ values of 38.24°, 44.15°, 64.44°, and 77.42° corresponding to the face-centered cubic (fcc) lattice of Ag (Supporting Information, Figure S25a,b).[16,63,64] The SEM images of derivative **3** in the presence of Ag^+ ions in H_2O/EtOH (8:2, v/v) solution showed the formation of nanoclusters on the surface of the aggregates of **3** (Figure 4A,B). The result of energy-dispersive X-ray (EDX) showed the presence of the Ag element, in which the peaks located between 2 and 4 keV are directly related to the characteristic K and L lines of silver (Supporting Information, Figure S26). The TEM images of the sample having a 1:1 ratio of aggregates of derivative **3** and Ag^+ ions showed larger nanoparticles (Figure 4C,D), although a

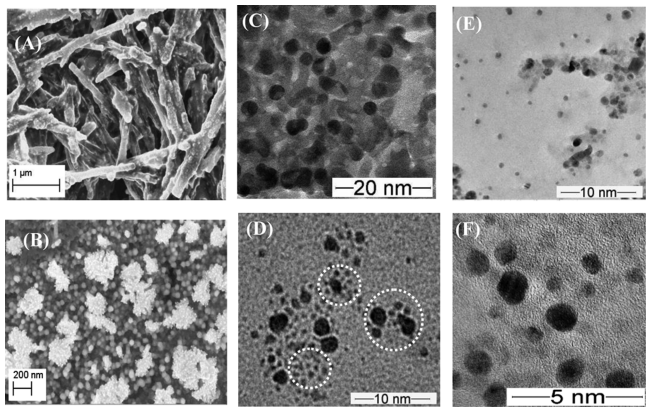

Figure 4. (A) SEM images of aggregates of derivative **3** on the addition of Ag^+ ions and (B) in the presence of Ag NCs. (C−F) TEM images showing Ag nanoclusters: (C, D) sample prepared by mixing aggregates of **3** and Ag^+ ions in 1:1 ratio, the circles showing the aggregates of clusters, and (E, F) sample prepared by mixing aggregates of **3** and Ag^+ ions in 1:2 ratio.

DOI: 10.1021/acsami.5b04377
ACS Appl. Mater. Interfaces 2015, 7, 22786−22795

Scheme 2. Probable Schematic Presentation of Formation of the Silver Nanocluster (Ag_7 NCs) from the Mixture of Ag^+ Ions and the Aggregates of Derivative 3 in H_2O/EtOH (8:2, v/v)

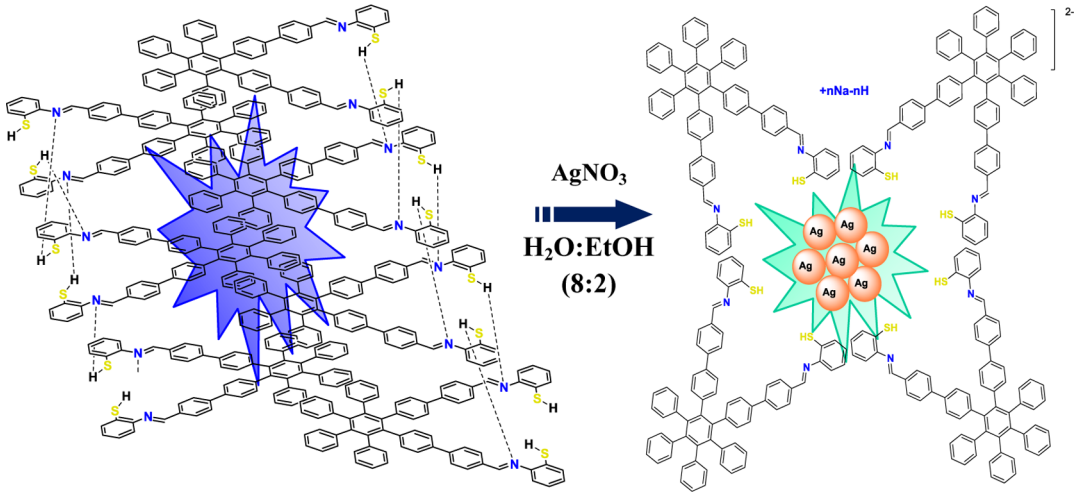

solution of aggregates of **3** in the presence of silver ions in 1:2 ratio showed the presence of smaller-sized particles (diameters range from 0.6 to 1.8 nm and average diameter ~1.1 nm); thus, lattice spacing was not clear (Figure 4E,F and Supporting Information, Figure S27a,b).[65,66] For the selected-area electron diffraction (SAED) pattern, the diffraction rings can be indexed as (111), (200), (220), (311), and (222) reflections of the fcc lattice of silver nanoclusters (Supporting Information, Figure S27c).[59] Further, the Raman-scattering spectrum of Ag NCs (1:2) suggests that peaks located at 614, 774, 1184, 1312, 1362, 1510, 1572, and 1650 cm^{-1} are corresponding to derivative **3** and peaks located at 269, 147, and 52 cm^{-1} belong to Ag NCs (Supporting Information, Figure S28).[67,68] From these results, we may conclude that there is a partial interaction between the aggregates of derivative **3** and Ag^+ ions when mixed in a 1:1 ratio, showing incomplete conversion to Ag NCs, but upon changing the ratio to 1:2, complete conversion was observed and much smaller sized Ag NCs (≤2 nm) were formed. Thus, the fluorescent supramolecular aggregates of derivative **3** function as reactors and stabilizers for the preparation of blue luminescent silver nanoclusters at room temperature.

2.6. Characterization of Silver Nanocluster (Ag_7 NCs) by ESI-MS Analysis. A molecular ion peak was found at m/z 2291.8297 (labeled i; see Supporting Information, Figure S29a) as a member of one isotope cluster among a series of similar, less-intense clusters that are spaced regularly (labeled i–vii) in the ESI-MS spectrum (in the negative ion mode) of silver nanoclusters (Supporting Information, Figure S29). The 0.5 spacing of the isotopes indicates that the ionized clusters bear −2 charge (z); the m/z values of the peaks therefore represent true molecular ion mass, which for the base peak of 2291.8297 correlate very well with the theoretical exact mass of $[Ag_7L_4]^{2-}$ (theoretical molecular weight 2291.8236, deviation 0.0061, where L = $C_{68}H_{48}N_2S_2$, FW 956.3259). This arrangement is supported by the excellent match of the theoretical and experimental isotopic distributions (Supporting Information, Figure S29b,c). The surrounding peaks (Supporting Information, Figure S29a) correspond to the following ions: $[Ag_7L_4 - H + Na]^{2-}$ (2301.4625, labeled ii), $[Ag_7L_4 - 2H + 2Na]^{2-}$ (2312.8051, labeled iii), $[Ag_7L_4 - 3H + 3Na]^{2-}$ (2323.2959, labeled iv), $[Ag_7L_4 - 4H + 4Na]^{2-}$ (2334.7870, labeled v), $[Ag_7L_4 - 5H + 5Na]^{2-}$ (2345.7780, labeled vi), $[Ag_7L_4 - 6H + 6Na]^{2-}$ (2356.7690, labeled vii). The assignments are also supported by their isotopic distribution patterns as well as the 11 Da spacing $[(m\mathrm{Na} - m\mathrm{H})/z]$. The ESI-MS experiments confirmed that the cluster is composed of seven silver atoms.[50,52] These results suggest that the silver ions interacted within the aggregates of derivative **3**, resulting in the formation of Ag_7 NCs (Scheme 2).

2.7. Purification of Ag NCs by the Phase Transfer Method. Further, the solution of in situ generated Ag NCs (≤2 nm) may also contain silver nanoparticles (plasmon particles of >2 nm, nonfluorescent) and silver ions. The separation of the silver nanoparticle impurities was achieved by the phase transfer method (Figure 5A,B).[69] The addition of toluene followed by vigorous shaking resulted in the separation of the nanoclusters from the nanoparticles. The yellow silver nanoclusters were transferred to the toluene phase (upper layer), the black silver nanoparticles were transferred to the interface of water–toluene, and the silver ions remained in the water phase (Figure 5C,D). After one phase transfer cycle, we carried out fluorescence studies of the toluene phase, and an enhancement of 1.8-fold was observed. This result indicates the separation of Ag NCs from Ag NPs.

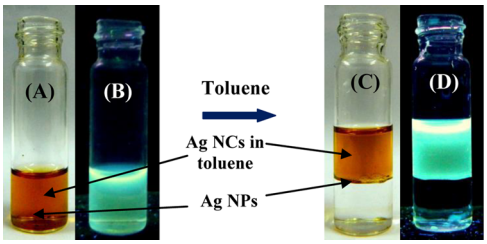

Figure 5. (Left) Aqueous solution of silver nanoclusters and nanoparticles under visible light (A) and under 365 nm UV light (B). (Right) After addition of toluene phase and shaking, the nanoparticles are located at the interface and the nanoclusters are located in the toluene phase (upper phase) under visible light (C) and under 365 nm UV light (D).

2.8. Catalytic Activity of Ag NCs for the Synthesis of Pyrroles. Having characterized the Ag NCs, we then examined the catalytic activity of the in situ generated Ag NCs in the cocyclization reaction of terminal alkynes (**4a–h**) with

DOI: 10.1021/acsami.5b04377
ACS Appl. Mater. Interfaces 2015, 7, 22786–22795

isocyanides (**5**) for the preparation of pyrroles.[3] To investigate the catalytic efficiency of in situ generated Ag NCs, we begin with the reaction of **4a** and **5** as a model reaction (Scheme 3).

Scheme 3. Cycloaddition of Alkynes 4a−h and Ethyl 2-Isocyanoacetate (5)[a]

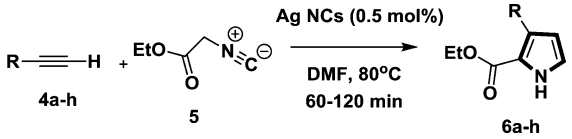

[a]Reaction conditions: **4a−h** (1 mmol), **5** (1.5 mmol) and Ag NCs (0.5 mol %) as a catalyst in DMF (3 mL) at 80°C under N_2 atmosphere for 60−120 min.

The reaction between 1 mmol of phenylacetylene (**4a**) and 1.5 mmol of ethyl 2-isocyanoacetate (**5**) in *N*,*N*-dimethylformamide (DMF) at 80 °C in the presence of 0.5 mol % Ag NCs (100 μL, H_2O/EtOH, 8:2, v/v) furnished the target compound **6a** in 80% yield. Even lowering the reaction temperature to 50 °C did not reduce the yield of the target product; however, longer reaction time was required. To study the scope of the reaction, different types of alkynes were used. The results of these reactions are summarized in Table 1. Interestingly, in the presence of only 0.5 mol % Ag NCs, all these reactions proceeded smoothly with a variety of aryl-substituted terminal alkynes. Though the differences were minor, electron-rich alkynes generally gave higher yields of the products, while in case of alkynes with electron-deficient groups, lower yields were obtained. We believe that more efficient interaction of electron-rich alkynes with Ag NCs is the reason for the relatively higher yields obtained in the case of electron-rich alkynes. All the products were isolated and characterized by ^{1}H NMR and ^{13}C NMR spectroscopy (Supporting Information, Figures S34−S49). Thus, from a synthetic point of view, this protocol exemplifies a simple, efficient, and atom economic way to construct multifunctional heterocyclic compounds rapidly in good yields with high selectivity.

To investigate the catalytic efficiency of the in situ generated Ag NCs, we have used different concentrations of Ag NCs to carry out the cocyclization reaction of **4a** and **5** (see Supporting Information, Table S4). It was observed that when 0.5 mol % of Ag NCs was used, the yield was 80% with a turnover frequency (TOF) of 8 h^{-1} and the reaction was complete in 2 h. However, at a higher concentration of Ag NCs (1 mol %), the yield was 81% in 2 h with a TOF of 4.05 h^{-1}. At a lower concentration of Ag NCs (0.1 mol %), the yield was 72% in 12 h with a TOF of 6 h^{-1}. From the above discussion, it is clear that the best results are obtained when 0.5 mol % of Ag NCs is used. The use of catalyst in such an extremely small quantity has never been successful for cocyclization reactions before the present study. Further, we have used 0.5 mol % of Ag NCs prepared by mixing the aggregates of derivative **3** and Ag^+ ions in 1:2 ratios for the preparation of pyrrole **6a**, but no significant change was observed in catalytic efficiency of Ag NCs with the sample prepared by mixing the aggregates of derivative **3** and Ag^+ ions in 1:1 ratios (Supporting Information, Table S4, entry 7).

2.9. Mechanism of Pyrroles Synthesis Catalyzed by Ag NCs. A probable reaction mechanism for the synthesis of pyrroles is given in Scheme 4. In the presence of Ag NCs catalyst, Ag NCs−acetylide complex (**7**) and Ag NCs−isocyanide complex (**8**) are formed. Subsequently, the cycloaddition between complexes **7** and **8** afford the key intermediate complex **9**. Finally, protonation followed by tautomerization furnish the pyrrole derivatives (**6a−h**). Further, the reusability of the Ag NCs catalyst was investigated under the conditions as given in Table 1 (entry 1). In the first cycle, the products were obtained in quantitative yields with complete conversion of reactants. Further, the resulting reaction mixture containing Ag NCs catalysts was then exposed to the same reaction for the next catalytic sequence by adding phenylacetylene (**4a**) and ethyl 2-isocyanoacetate (**5**), and it was observed that the Ag NCs can be reused as catalysts at least three times without significant loss of catalytic activity.

3. CONCLUSIONS

To conclude, a hexaphenylbenzene-based derivative **3** appended with thiol moieties has been designed and synthesized that exhibited AIEE characteristics and formed rodlike fluorescent aggregates in mixed aqueous media. These aggregates served as reactors and stabilizers for the formation of well-defined, monodisperse, blue luminescent silver nanoclusters (Ag_7 NCs) in aqueous medium at room temperature. These in situ generated silver nanoclusters showed excellent catalytic activity in the click synthesis of pyrroles (**6a−h**) by the cocyclization of terminal alkynes and isocyanides.

4. EXPERIMENTAL SECTION

4.1. General Experimental Methods and Materials.[12] The general experimental methods, quantum yield calculations, and materials used are same as reported earlier by us.[12] The TEM images were recorded using a HR-TEM-JEM 2100 microscope. The FT-IR spectra were recorded using a VARIAN 660 IR spectrometer. Raman spectra were recorded with a Raneshaw inVia reflex micro-Raman microscope.

4.2. UV−Vis and Fluorescence Titrations.[12] A 0.956 mg portion of compound **3** was dissolved in 1.0 mL of dry THF to prepare 1.0 mL of 10^{-3} M stock solution; 15 μL of this stock solution was further diluted with 585 μL of EtOH and 2.4 mL of HEPES buffer (0.05 M, pH 7.05) to prepare 3 mL of 5.0 μM solution of derivative **3** in H_2O/EtOH (8:2, v/v), and this solution was used for each UV−vis and fluorescence experiment. Aliquots of freshly prepared standard

Scheme 4. Proposed Mechanism for the Silver-Nanocluster-Catalyzed Cycloaddition of Terminal Alkynes (4a−h) with Ethyl 2-Isocyanoacetate (5)

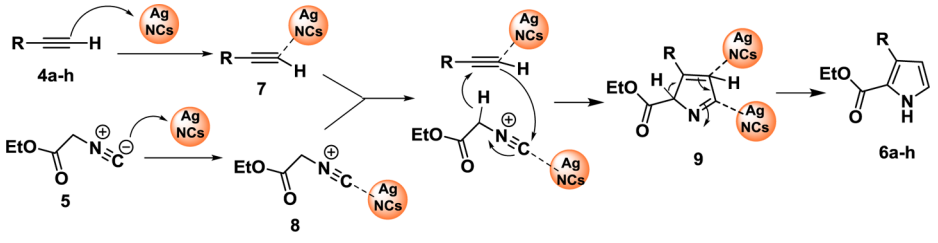

DOI: 10.1021/acsami.5b04377
ACS Appl. Mater. Interfaces 2015, 7, 22786−22795

solutions of metal perchlorates [$M(ClO_4)_x$; M = Ag^+, Hg^{2+}, Au^{3+}, Zn^{2+}, Cu^{2+}, Fe^{2+}, Fe^{3+}, Co^{2+}, Pb^{2+}, Ni^{2+}, Pd^{2+}, Cd^{2+}, Ba^{2+}, Mg^{2+}, and Al^{3+}; x = 1−3] and metal chlorides (MCl_Y; Y = 1−3) in distilled water and $AgNO_3$ in EtOH (10^{-1}−10^{-3} M) were added to 3 mL solution of compound **3** in quartz cuvettes and spectra were recorded.

4.3. Synthesis of Silver Nanoclusters. *Sample Prepared in 1:1 Ratio.* To 1.0 mL of compound **3** solution (0.15 mM) in H_2O/EtOH (8:2, v/v) was added 1.0 mL of an aqueous solution of $AgNO_3$ (0.15 mM). The reaction mixture was stirred at room temperature, and after 1.5 h, the color of the solution mixture changed from colorless to yellow, which gradually darkened within 4 h, and thereafter, the formation of luminescent silver nanoclusters takes place.

Sample Prepared in 1:2 Ratio. To 1.0 mL of compound **3** solution (0.075 mM) in H_2O/EtOH (8:2, v/v) was added 1.0 mL of an aqueous solution of $AgNO_3$ (0.15 mM). The reaction mixture was stirred at room temperature, and after 1 h, the color of solution mixture changed from colorless to yellow, which gradually darkened within 4 h, and thereafter, the formation of luminescent silver nanoclusters takes place.

A 100 μL (0.5 mol %) portion of this Ag NCs solution was used as a catalyst in each reaction.

4.4. Synthesis of HPB Derivative 3. To a solution of 2-aminothiophenol **2** (0.018 g, 0.148 mmol) in THF:EtOH 4:6 (10 mL) was added a solution of HPB aldehyde **1**[10] (0.05 g, 0.067 mmol) in THF:EtOH 4:6 (10 mL). The reaction mixture was stirred at 80 °C for 10 min, and thereafter, it turned turbid. The reaction mixture was cooled and methanol was added to separate a solid, which was filtered and recrystallized from methanol to afford the colorless compound **3** in 89% yield (0.058 g) (Scheme 1): mp >280 °C; ^{1}H NMR (500 MHz, $CDCl_3$, ppm) δ = 8.78 (s, 2H, HC═N), 8.24 (d, J = 10 Hz, 2H, ArH), 8.07 (d, J = 10 Hz, 4H, ArH), 7.91 (d, J = 10 Hz, 2H, ArH), 7.84 (t, J = 10 Hz, 2H, ArH), 7.59 (d, J = 10 Hz, 4H, ArH), 7.50 (t, J = 7.5 Hz, 2H, ArH), 7.39 (t, J = 7.5 Hz, 2H, ArH), 7.25 (d, J = 10 Hz, 4H, ArH), 7.08 (t, J = 7.5 Hz, 2H, ArH), 7.00 (d, J = 10 Hz, 4H, ArH), 6.91−6.89 (m, 16H, ArH) 3.52 (s, 2H, SH); ^{13}C NMR (125 MHz, $CDCl_3$, ppm) δ = 160.9, 156.7 (HC═N), 143.2, 140.4, 136.8, 136.4, 132.1, 131.4, 130.1, 128.1, 127.8, 127.2, 126.8, 126.6, 125.6, 125.3, 123.1, 118.2; ESI-MS calcd for $C_{68}H_{48}N_2S_2$ 979.3151, found m/z 979.4329 $[M + Na]^+$; FT-IR (KBr) ν_{max} (cm^{-1}) = 1602 (>C═N) and 2580 (−SH). Anal. Calcd for $C_{68}H_{48}N_2S_2$: C, 85.32; H, 5.05; N, 2.93. Found: C, 85.33%; H, 5.04%; N, 2.92%.

4.5. General Procedure for the Preparation of Pyrrole. A mixture of arylalkynes **4a**−**h** (1 mmol), ethyl 2-isocyanoacetate (**5**) (1.5 mmol), and Ag NCs (0.5 mol %) as a catalyst in DMF (3 mL) was stirred at 80 °C for 1−2 h under N_2 atmosphere. After the completion of the reaction (TLC), the solvent was removed under reduced pressure to obtain a residue to which water was added. The aqueous layer was extracted with chloroform (3 × 20 mL). The combined chloroform fractions were washed with water, dried over anhydrous Na_2SO_4, and distilled under reduced pressure to yield a solid residue. The pyrrole derivatives **6a**−**h** were thus isolated in good yields by column chromatography using hexane/ethyl acetate (8:2) as an eluent. The structures of all the compounds (**6a**−**h**) were confirmed from their spectroscopic and analytical data (Supporting Information, Figures S34−S49).

*Compound **6a**.* ^{1}H NMR (300 MHz, $CDCl_3$, ppm) δ = 9.86 (s, 1H, NH), 7.51 (d, J = 6 Hz, 2H, ArH), 7.40−7.31 (m, 3H, ArH), 7.02 (t, J = 4.5 Hz, 1H, ArH), 6.38 (t, J = 4.5 Hz, 1H, ArH), 4.28 (q, J = 4.5 Hz, 2H, O−CH_2−CH_3), 1.31 (t, J = 6 Hz, 3H, O−CH_2−CH_3); ^{13}C NMR (75 MHz, $CDCl_3$, ppm) δ = 169.0 (CO), 139.6, 139.2, 132.1, 128.7, 128.5, 128.2, 122.1, 120.2, 117.2, 114.0, 60.2, 14.1.

*Compound **6b**.* ^{1}H NMR (300 MHz, $CDCl_3$, ppm) δ = 10.02 (s, 1H, NH), 7.45 (d, J = 6 Hz, 1H, ArH), 7.34 (d, J = 6 Hz, 1H, ArH), 4.98 (q, J = 9 Hz, 2H, O−CH_2−CH_3), 1.45 (t, J = 3 Hz, 3H, O−CH_2−CH_3), 0.27 (s, 9H, $SiMe_3$); ^{13}C NMR (75 MHz, $CDCl_3$, ppm) δ = 161.7 (CO), 133.3, 131.7, 131.4, 123.1, 51.0, 14.1.

*Compound **6c**.* ^{1}H NMR (300 MHz, $CDCl_3$, ppm) δ = 11.02 (s, 1H, OH), 9.86 (s, 1H, NH), 7.64 (d, J = 6 Hz, 1H, ArH), 7.53 (d, J = 6 Hz, 1H, ArH), 4.26 (q, J = 3 Hz, 2H, O−CH_2−CH_3), 1.38 (t, J = 4.5 Hz, 3H, O−CH_2−CH_3), 1.30 (s, 6H, $HOCMe_2$); ^{13}C NMR (75 MHz, $CDCl_3$, ppm) δ = 166.6 (CO), 138.6, 134.6, 128.6, 126.0, 62.4, 60.5, 30.6, 14.3.

*Compound **6d**.* ^{1}H NMR (300 MHz, $CDCl_3$, ppm) δ = 9.89 (s, 1H, NH), 7.78 (d, J = 6 Hz, 1H, ArH), 7.50 (d, J = 6 Hz, 2H, ArH), 7.38 (d, J = 6 Hz, 2H, ArH), 7.00 (d, J = 9 Hz, 1H, ArH), 4.10 (q, J = 3 Hz, 2H, O−CH_2−CH_3), 1.81 (t, J = 3 Hz, 3H, O−CH_2−CH_3); ^{13}C NMR (75 MHz, $CDCl_3$, ppm) δ = 174.8 (CO), 138.7, 137.2, 131.8, 128.6, 126.1, 116.6, 113.8, 49.2, 17.4.

*Compound **6e**.* ^{1}H NMR (300 MHz, $CDCl_3$, ppm) δ = 9.74 (s, 1H, NH), 7.86 (d, J = 6 Hz, 1H, ArH), 7.74 (d, J = 6 Hz, 2H, ArH), 7.53 (d, J = 6 Hz, 2H, ArH), 6.73 (d, J = 2 Hz, 1H, ArH), 4.16 (q, J = 6 Hz, 2H, O−CH_2−CH_3), 1.11 (t, J = 7.5 Hz, 3H, O−CH_2−CH_3); ^{13}C NMR (75 MHz, $CDCl_3$, ppm) δ = 166.6 (CO), 149.0, 137.6, 134.1, 129.6, 126.0, 123.2, 117.4, 107.9, 62.3, 17.5.

*Compound **6f**.* ^{1}H NMR (300 MHz, $CDCl_3$, ppm) δ = 10.18 (s, 1H, NH), 7.90 (d, J = 3 Hz, 1H, ArH), 7.57 (d, J = 3 Hz, 2H, ArH), 7.46 (d, J = 3 Hz, 2H, ArH), 7.21 (d, J = 3 Hz, 1H, ArH), 4.15 (q, J = 4.5 Hz, 2H, O−CH_2−CH_3), 3.85 (s, 3H, OMe), 1.26 (t, J = 3 Hz, 3H, O−CH_2−CH_3); ^{13}C NMR (75 MHz, $CDCl_3$, ppm) δ = 174.9 (CO), 138.6, 137.9, 136.1, 128.2, 126.0, 123.5, 112.0, 62.2, 60.3, 17.5.

*Compound **6g**.* ^{1}H NMR (300 MHz, $CDCl_3$, ppm) δ = 9.49 (s, 1H, NH), 7.95 (d, J = 6 Hz, 1H, ArH), 7.68 (d, J = 6 Hz, 2H, ArH), 7.48 (d, J = 6 Hz, 2H, ArH), 6.70 (d, J = 6 Hz, 1H, ArH), 4.31 (q, J = 4.5 Hz, 2H, (O−CH_2−CH_3), 2.79 (s, 3H, CH_3) 1.32 (t, J = 4.5 Hz, 3H, (O−CH_2−CH_3); ^{13}C NMR (75 MHz, $CDCl_3$, ppm) δ = 166.6 (CO), 139.1, 138.7, 137.6, 134.1, 128.8, 126.0, 123.6, 123.2, 117.4, 60.5, 30.6, 17.5.

*Compound **6h**.* ^{1}H NMR (300 MHz, $CDCl_3$, ppm) δ = 9.67 (s, 1H, NH), 7.86 (d, J = 9 Hz, 1H, ArH), 7.63 (d, J = 6 Hz, 2H, ArH), 7.48 (d, J = 6 Hz, 2H, ArH), 6.60 (d, J = 6 Hz, 1H, ArH), 5.83 (s, 2H, NH_2), 4.98 (q, J = 9 Hz, 2H, (O−CH_2−CH_3), 1.31 (t, J = 6 Hz, 3H, (O−CH_2−CH_3); ^{13}C NMR (75 MHz, $CDCl_3$, ppm) δ = 162.5 (CO), 144.9, 134.0, 129.6, 125.9, 123.1, 117.3, 107.9, 60.4 (O−CH_2−CH_3), 14.2 (O−CH_2−CH_3).

■ ASSOCIATED CONTENT

Supporting Information

The Supporting Information is available free of charge on the ACS Publications website at DOI: 10.1021/acsami.5b04377.

^{1}H and ^{13}C NMR spectra, mass spectra, and IR spectra of compounds **3** and **6a**−**h**; UV−vis and fluorescence studies; detection limits; SEM and TEM images; powder XRD analysis; DLS studies; Raman scattering patterns; table of comparison of catalytic activity of the present system with those in the literature (Figures S1−S49 and Tables S1−S6) (PDF)

■ AUTHOR INFORMATION

Corresponding Authors

*V.B. e-mail: vanmanan@yahoo.co.in.

*M.K. e-mail: mksharmaa@yahoo.co.in.

Notes

The authors declare no competing financial interest.

■ ACKNOWLEDGMENTS

M.K. and V.B. are thankful to Science and Engineering Research Board (SERB), New Delhi (ref no. SR/S1/OC-69/2012 and EMR/2014/000149, respectively) for financial support. S.P. is thankful to UGC (New Delhi) for a Senior Research Fellowship (SRF). We are thankful to Dr. Atul Khanna and Mr. Ravinder Singh for the Raman spectral analysis and TEM study, respectively. We are also thankful to UGC (New Delhi) for the "University with Potential for Excellence" (UPE) project.

DOI: 10.1021/acsami.5b04377
ACS Appl. Mater. Interfaces 2015, 7, 22786−22795

REFERENCES

(1) Gottesfeld, J. M.; Neely, L.; Trauger, J. W.; Baird, E. E.; Dervan, P. B. Regulation of Gene Expression by Small Molecules. *Nature* **1997**, *387*, 202−205.

(2) Minetto, G.; Raveglia, L. F.; Taddei, M. Microwave-Assisted Paal-Knorr Reaction: A Rapid Approach to Substituted Pyrroles and Furans. *Org. Lett.* **2004**, *6*, 389−392.

(3) Gao, M.; He, C.; Chen, H.; Bai, R.; Cheng, B.; Lei, A. Synthesis of Pyrroles by Click Reaction: Silver-Catalyzed Cycloaddition of Terminal Alkynes with Isocyanides. *Angew. Chem., Int. Ed.* **2013**, *52*, 6958−6961.

(4) Li, B.; Wang, N.; Liang, Y.; Xu, S.; Wang, B. Ruthenium-Catalyzed Pyrrole Synthesis via Oxidative Annulation of Enamides and Alkynes. *Org. Lett.* **2013**, *15*, 136−139.

(5) Bhalla, V.; Gupta, A.; Kumar, M. Nanoaggregates of a Pentacenequinone Derivative as Reactors for the Preparation of Palladium Nanoparticles. *Chem. Commun.* **2012**, *48*, 11862−11864.

(6) Sharma nee Kamaldeep, K.; Kaur, S.; Bhalla, V.; Kumar, M.; Gupta, A. Pentacenequinone Derivatives for Preparation of Gold Nanoparticles: Facile Synthesis and Catalytic Application. *J. Mater. Chem. A* **2014**, *2*, 8369−8375.

(7) Kaur, S.; Bhalla, V.; Kumar, M. Copper Nanoparticles Generated from Aggregates of a Hexarylbenzene Derivative: a Reusable Catalytic System for 'Click' Reactions. *Chem. Commun.* **2015**, *51*, 526−529.

(8) Kaur, S.; Bhalla, V.; Kumar, M. AIEE Active Perylene Bisimide Supported Mercury Nanoparticles for Synthesis of Amides via Aldoximes/Ketoximes Rearrangement. *Chem. Commun.* **2015**, *51*, 4085−4088.

(9) Pramanik, S.; Bhalla, V.; Kumar, M. A Hexaphenylbenzene Based AIEE Active Probe for the Preparation of Ferromagnetic α-Fe_2O_3 Nanoparticles: Facile Synthesis and Catalytic Applications. *Chem. Commun.* **2014**, *50*, 13533−13536.

(10) Sharma, K.; Singh, G.; Singh, G.; Kumar, M.; Bhalla, V. Silver Nanoparticles: Facile Synthesis and Their Catalytic Application for the Degradation of Dyes. *RSC Adv.* **2015**, *5*, 25781−25788.

(11) Bhalla, V.; Pramanik, S.; Kumar, M. Cyanide Modulated Fluorescent Supramolecular Assembly of a Hexaphenylbenzene Derivative for Detection of Trinitrotoluene at the Attogram level. *Chem. Commun.* **2013**, *49*, 895−857.

(12) Pramanik, S.; Bhalla, V.; Kumar, M. Hexaphenylbenzene-Based Fluorescent Aggregates for Ratiometric Detection of Cyanide Ions at Nanomolar Level: Set-Reset Memorized Sequential Logic Device. *ACS Appl. Mater. Interfaces* **2014**, *6*, 5930−5939.

(13) Gan, W.; Xu, B.; Dai, H.-L. Activation of Thiols at a Silver Nanoparticle Surface. *Angew. Chem., Int. Ed.* **2011**, *50*, 6622−6625.

(14) Yu, J.; Patel, S. A.; Dickson, R. M. In Vitro and Intracellular Production of Peptide-Encapsulated Fluorescent Silver Nanoclusters. *Angew. Chem., Int. Ed.* **2007**, *46*, 2028−2030.

(15) Diez, I.; Kanyuk, M. I.; Demchenko, A. P.; Walther, A.; Jiang, H.; Ikkala, O.; Ras, R. H. A. Blue, Green and Red Emissive Silver Nanoclusters Formed in Organic Solvents. *Nanoscale* **2012**, *4*, 4434−4437.

(16) Lu, Y.; Chen, W. Sub-Nanometre Sized Metal Clusters: From Synthetic Challenges to the Unique Property Discoveries. *Chem. Soc. Rev.* **2012**, *41*, 3594−3623.

(17) Lu, Y.; Chen, W. Size Effect of Silver Nanoclusters on Their Catalytic Activity for Oxygen Electro-Reduction. *J. Power Sources* **2012**, *197*, 107−110.

(18) Liu, M.; Chen, W. Green Synthesis of Silver Nanoclusters Supported on Carbon Nanodots: Enhanced Photoluminescence and High Catalytic Activity for Oxygen Reduction Reaction. *Nanoscale* **2013**, *5*, 12558−12564.

(19) Gao, S.; Chen, D.; Li, Q.; Ye, J.; Jiang, H.; Amatore, C.; Wang, X. Near-Infrared Fluorescence Imaging of Cancer Cells and Tumors Through Specific Biosynthesis of Silver Nanoclusters. *Sci. Rep.* **2014**, *4*, 4384.

(20) Udayabhaskararao, T.; Sun, Y.; Goswami, N.; Pal, S. K.; Balasubramanian, K.; Pradeep, T. Ag_7Au_6: A 13-Atom Alloy Quantum Cluster. *Angew. Chem., Int. Ed.* **2012**, *51*, 2155−2159.

(21) Shang, L.; Dong, S. Silver Nanocluster-based Fluorescent Sensors for Sensitive Detection of Cu(II). *J. Mater. Chem.* **2008**, *18*, 4636−4640.

(22) Chandirasekar, S.; Chandrasekaran, C.; Muthukumarasamyvel, T.; Sudhandiran, G.; Rajendiran, N. Sodium Cholate-Templated Blue Light-Emitting Ag Subnanoclusters: In Vivo Toxicity and Imaging in Zebrafish Embryos. *ACS Appl. Mater. Interfaces* **2015**, *7*, 1422−1430.

(23) Enkin, N.; Sharon, E.; Golub, E.; Willner, I. Ag Nanocluster/DNA Hybrids: Functional Modules for the Detection of Nitroaromatic and RDX Explosives. *Nano Lett.* **2014**, *14*, 4918−4922.

(24) Chen, Y.; Yang, T.; Pan, H.; Yuan, Y.; Chen, L.; Liu, M.; Zhang, K.; Zhang, S.; Wu, P.; Xu, J. Photoemission Mechanism of Water-Soluble Silver Nanoclusters: Ligand-to-Metal-Metal Charge Transfer vs Strong Coupling between Surface Plasmon and Emitters. *J. Am. Chem. Soc.* **2014**, *136*, 1686−1689.

(25) Yeh, H.-C.; Sharma, J.; Shih, I.-M.; Vu, D. M.; Martinez, J. S.; Werner, J. H. A Fluorescence Light-Up Ag Nanocluster Probe That Discriminates Single-Nucleotide Variants by Emission Color. *J. Am. Chem. Soc.* **2012**, *134*, 11550−11558.

(26) Roy, S.; Baral, A.; Banerjee, A. Tuning of Silver Cluster Emission from Blue to Red Using a Bio-Active Peptide in Water. *ACS Appl. Mater. Interfaces* **2014**, *6*, 4050−4056.

(27) Bertorelle, F.; Hamouda, R.; Rayane, D.; Broyer, M.; Antoine, R.; Dugourd, P.; Gell, L.; Kulesza, A.; Mitri, R.; Bona-Kouteck, V. Synthesis, Characterization and Optical Properties of low Nuclearity Liganded Silver Clusters: $Ag_{31}(SG)_{19}$ and $Ag_{15}(SG)_{11}$. *Nanoscale* **2013**, *5*, 5637−5643.

(28) He, X.; Wang, Y.; Gao, C.-Y.; Jiang, H.; Zhao, L. A Macrocycle-Assisted Nanoparticlization Process for Bulk Ag_2S. *Chem. Sci.* **2015**, *6*, 654−658.

(29) Yuan, Z.; Chen, Y.-C.; Li, H.-W.; Chang, H.-T. Fluorescent Silver Nanoclusters Stabilized by DNA Scaffold. *Chem. Commun.* **2014**, *50*, 9800−9815.

(30) Diez, I.; Ras, R. H. A. Fluorescent Silver Nanoclusters. *Nanoscale* **2011**, *3*, 1963−1970.

(31) Sharon, E.; Enkin, N.; Albada, H. B.; Willner, I. Aptasensors Based on Supramolecular Structures of Nucleic Acid-Stabilized Ag Nanoclusters. *Chem. Commun.* **2015**, *51*, 1100−1103.

(32) Neidig, M. L.; Sharma, J.; Yeh, H.-C.; Martinez, J. S.; Conradson, S. D.; Shreve, A. P. Ag K-Edge EXAFS Analysis of DNA-Templated Fluorescent Silver Nanoclusters: Insight into the Structural Origins of Emission Tuning by DNA Sequence Variations. *J. Am. Chem. Soc.* **2011**, *133*, 11837−11839.

(33) Guo, W.; Orbach, R.; Mironi-Harpaz, I.; Seliktar, D.; Willner, I. Fluorescent DNA Hydrogels Composed of Nucleic Acid-Stabilized Silver Nanoclusters. *Small* **2013**, *9*, 3748−3752.

(34) Sharma, J.; Rocha, R. C.; Phipps, M. L.; Yeh, H.-C.; Balatsky, K. A.; Vu, D. M.; Shreve, A. P.; Werner, J. H.; Martinez, J. S. A DNA-Templated Fluorescent Silver Nanocluster with Enhanced Stability. *Nanoscale* **2012**, *4*, 4107−4110.

(35) Copp, S. M.; Schultz, D.; Swasey, S.; Pavlovich, J.; Debord, M.; Chiu, A.; Olsson, K.; Gwinn, E. Magic Numbers in DNA-Stabilized Fluorescent Silver Clusters Lead to Magic Colors. *J. Phys. Chem. Lett.* **2014**, *5*, 959−963.

(36) Yeh, H.-C.; Sharma, J.; Han, J. J.; Martinez, J. S.; Werner, J. H. A DNA-Silver Nanocluster Probe That Fluoresces upon Hybridization. *Nano Lett.* **2010**, *10*, 3106−3110.

(37) Yang, C.; Shi, K.; Dou, B.; Xiang, Y.; Chai, Y.; Yuan, R. In Situ DNA-Templated Synthesis of Silver Nanoclusters for Ultrasensitive and Label-Free Electrochemical Detection of MicroRNA. *ACS Appl. Mater. Interfaces* **2015**, *7*, 1188−1193.

(38) AbdulHalim, L. G.; Bootharaju, M. S.; Tang, Q.; Del Gobbo, D.; AbdulHalim, R. G.; Eddaoudi, M.; Jiang, D.; Bakr, O. M. $Ag_{29}(BDT)_{12}(TPP)_4$: A Tetravalent Nanocluster. *J. Am. Chem. Soc.* **2015**, *137*, 11970−11975.

(39) Gao, S.; Chen, D.; Li, Q.; Ye, J.; Jiang, H.; Amatore, C.; Wang, X. Near-Infrared Fluorescence Imaging of Cancer Cells and Tumors Through Specific Biosynthesis of Silver Nanoclusters. *Sci. Rep.* **2014**, *4*, 4384.

DOI: 10.1021/acsami.5b04377
ACS Appl. Mater. Interfaces 2015, 7, 22786−22795

(40) Ma, J.-L.; Yin, B.-C.; Le, H.-N.; Ye, B.-C. Label-Free Detection of Sequence-Specific DNA Based on Fluorescent Silver Nanoclusters-Assisted Surface Plasmon-Enhanced Energy Transfer. *ACS Appl. Mater. Interfaces* **2015**, *7*, 12856−12863.
(41) Bootharaju, M. S.; Burlakov, V. M.; Besong, T. M. D.; Joshi, C. P.; AbdulHalim, L. G.; Black, D. M.; Whetten, R. L.; Goriely, A.; Bakr, O. M. Reversible Size Control of Silver Nanoclusters via Ligand-Exchange. *Chem. Mater.* **2015**, *27*, 4289−4297.
(42) Chandirasekar, S.; Chandrasekaran, C.; Muthukumarasamyvel, T.; Sudhandiran, G.; Rajendiran, N. Sodium Cholate-Templated Blue Light-Emitting Ag Subnanoclusters: In Vivo Toxicity and Imaging in Zebrafish Embryos. *ACS Appl. Mater. Interfaces* **2015**, *7*, 1422−1430.
(43) Zhang, J.; Dong, W.; Qiao, L.; Li, J.; Zheng, J.; Sheng, J. Silver Nanocluster Formation in Soda-lime Silicate Glass by X-ray Irradiation and Annealing. *J. Cryst. Growth* **2007**, *305*, 278−284.
(44) Wang, Y.; Sun, Q.; Zhu, L.; Zhang, J.; Wang, F.; Lu, L.; Yu, H.; Xu, Z.; Zhang, W. Triplex Molecular Beacons for Sensitive Recognition of Melamine based on a Basic-Site Containing DNA and Fluorescent Silver Nanoclusters. *Chem. Commun.* **2015**, *51*, 7958−7961.
(45) Chen, L.; Sha, L.; Qiu, Y.; Wang, G.; Jiang, H.; Zhang, X. An Amplified Electrochemical Aptasensor Based on Hybridization Chain Reactions and Catalysis of Silver Nanoclusters. *Nanoscale* **2015**, *7*, 3300−3308.
(46) Zhang, Y.; Zhu, C.; Zhang, L.; Tan, C.; Yang, J.; Chen, B.; Wang, L.; Zhang, H. DNA-Templated Silver Nanoclusters for Multiplexed Fluorescent DNA Detection. *Small* **2015**, *11*, 1385−1390.
(47) Pal, N. K.; Kryschi, C. A Facile Synthesis of Highly Stable and Luminescent Ag clusters: A Steady-State and Time-Resolved Spectroscopy Study. *Phys. Chem. Chem. Phys.* **2015**, *17*, 1957−1965.
(48) Kubota, Y.; Tanaka, S.; Funabiki, K.; Matsui, M. Synthesis and Fluorescence Properties of Thiazole-Boron Complexes Bearing a β-Ketoiminate Ligand. *Org. Lett.* **2012**, *14*, 4682−4685.
(49) Muhammed, M. A. H.; Aldeek, F.; Palui, G.; Trapiella-Alfonso, L.; Mattoussi, H. Growth of In Situ Functionalized Luminescent Silver Nanoclusters by Direct Reduction and Size Focusing. *ACS Nano* **2012**, *6*, 8950−8961.
(50) Udaya Bhaskara Rao, T.; Pradeep, T. Luminescent Ag_7 and Ag_8 Clusters by Interfacial Synthesis. *Angew. Chem., Int. Ed.* **2010**, *49*, 3925−3929.
(51) Xu, H.; Suslick, K. S. Water-Soluble Fluorescent Silver Nanoclusters. *Adv. Mater.* **2010**, *22*, 1078−1082.
(52) Wu, Z.; Lanni, E.; Chen, W.; Bier, M. E.; Ly, D.; Jin, R. High Yield, Large Scale Synthesis of Thiolate-Protected Ag_7 Clusters. *J. Am. Chem. Soc.* **2009**, *131*, 16672−16674.
(53) Zhang, J.; Xu, S.; Kumacheva, E. Photogeneration of Fluorescent Silver Nanoclusters in Polymer Microgels. *Adv. Mater.* **2005**, *17*, 2336−2340.
(54) Xie, W. Y.; Huang, W. T.; Li, N. B.; Luo, H. Q. Silver(I) Ions and Cysteine Detection Based on Photoinduced Electron Transfer Diated by Cytosine-Ag^+ Cytosine Base Pairs. *Analyst* **2011**, *136*, 4130−4133.
(55) Sun, W.; Yao, J.; Yao, T.; Shi, S. Label-free Fluorescent DNA Sensor for the Detection of Silver Ions Based on Molecular Light Switch Ru Complex and Unmodified Quantum Dots. *Analyst* **2013**, *138*, 421−424.
(56) Velázquez, J. J.; Tikhomirov, V. K.; Chibotaru, L. F.; Cuong, N. T.; Kuznetsov, A. S.; Rodríguez, V. D.; Nguyen, M. T.; Moshchalkov, V. V. Energy Level Diagram and Kinetics of Luminescence of Ag Nanoclusters Dispersed in a Glass Host. *Opt. Express* **2012**, *20*, 13582−13591.
(57) Ganguly, M.; Pal, J.; Mondal, C.; Pal, A.; Pal, T. Imine (−CH═N−) brings Selectivity for Silver Enhanced Fluorescence. *Dalton Trans.* **2015**, *44*, 4370−4379.
(58) Wang, Y.-L.; Nan, F.; Liu, X.-L.; Zhou, L.; Peng, X.-N.; Zhou, Z.-K.; Yu, Y.; Hao, Z.-H.; Wu, Y.; Zhang, W.; Wang, Q.-Q.; Zhang, Z. Plasmon-Enhanced Light Harvesting of Chlorophylls on Near-Percolating Silver Films via One-Photon Anti-Stokes Upconversion. *Sci. Rep.* **2013**, *3*, 1861.
(59) Wei, W.; Lu, Y.; Chen, W.; Chen, S. One-Pot Synthesis, Photoluminescence, and Electrocatalytic Properties of Subnanometer-Sized Copper Clusters. *J. Am. Chem. Soc.* **2011**, *133*, 2060−2063.
(60) Gao, X.; Lu, Y.; Liu, M.; He, S.; Chen, W. Sub-Nanometer Sized $Cu_6(GSH)_3$ Clusters: One-Step Synthesis and Electrochemical Detection of Glucose. *J. Mater. Chem. C* **2015**, *3*, 4050−4056.
(61) Wang, Y.; Dai, C.; Yan, X.-P. Fabrication of Folate Bioconjugated Near-Infrared Fluorescent Silver Nanoclusters for Targeted in Vitro and in Vivo Bioimaging. *Chem. Commun.* **2014**, *50*, 14341−14344.
(62) Woehrle, G. H.; Warner, M. G.; Hutchison, J. E. Ligand Exchange Reactions Yield Subnanometer, Thiol-Stabilized Gold Particles with Defined Optical Transitions. *J. Phys. Chem. B* **2002**, *106*, 9979−9981.
(63) Adhikari, B.; Banerjee, A. Facile Synthesis of Water-Soluble Fluorescent Silver Nanoclusters and Hg^{II} Sensing. *Chem. Mater.* **2010**, *22*, 4364−4371.
(64) Wu, Z.; Chen, J.; Jin, R. One-Pot Synthesis of $Au_{25}(SG)_{18}$ 2- and 4-nm Gold Nanoparticles and Comparison of Their Size-Dependent Properties. *Adv. Funct. Mater.* **2011**, *21*, 177−183.
(65) Chen, W.-T.; Hsu, Y.-J.; Kamat, P. V. Realizing Visible Photoactivity of Metal Nanoparticles: Excited-State Behavior and Electron-Transfer Properties of Silver (Ag_8) Clusters. *J. Phys. Chem. Lett.* **2012**, *3*, 2493−2499.
(66) Liu, G.; Feng, D.-Q.; Mu, X.; Zheng, W.; Chen, T.; Qi, L.; Li, D. DNA-Functionalized Silver Nanoclusters as a Chemopalette: Tunable Fluorescence for Turn-on Detection of Cysteine. *J. Mater. Chem. B* **2013**, *1*, 2128−2131.
(67) Xu, S.; Wang, Z.; Wang, C.; Wang, Z.; Cui, Y. Investigation of a Naked Ag_7 cluster: Configurations and Spectral Characteristics. *New J. Chem.* **2015**, *39*, 3105−3108.
(68) Upender, G.; Satyavathi, R.; Raju, B.; Shadak Alee, K.; Narayana Rao, D.; Bansal, C. Silver Nanocluster Films as Novel SERS Substrates for Ultrasensitive Detection of Molecules. *Chem. Phys. Lett.* **2011**, *511*, 309−314.
(69) Yuan, X.; Luo, Z.; Zhang, Q.; Zhang, X.; Zheng, Y.; Lee, J. Y.; Xie, J. Synthesis of Highly Fluorescent Metal (Ag, Au, Pt, and Cu) Nanoclusters by Electrostatically Induced Reversible Phase Transfer. *ACS Nano* **2011**, *5*, 8800−8808.

DOI: 10.1021/acsami.5b04377
ACS Appl. Mater. Interfaces 2015, 7, 22786−22795